Timing of initiation of extension in the Tianshan, based on structural, geochemical and geochronological analyses of bimodal volcanism and olistostrome in the Bogda Shan (NW China)

Liangshu Shu [1,*], Bo Wang [1,2], Wenbin Zhu [1], Zhaojie Guo [3], Jaques Charvet [4], Yuan Zhang [1]

1, State Key Laboratory for Mineral Deposits Research, Nanjing University, Nanjing 210093, China;

2, Institute of Earth Sciences, Academia Sinica, Nankang, Taipei, 11529 Taiwan;

3, School of Earth and Space Sciences, Peking University, Beijing 100871, China;

4, Institut des Sciences de la Terre d'Orléans,UMR 6113, 1A rue de la Férollerie, 45100 Orléans, France

** Corresponding author: LS Shu:*

Email: lsshu2003@yahoo.com.cn

Revised V2 submitted to ***International Journal of Earth Sciences***

First submission on Oct. 21, 2009

Abstract: This paper describes an olistostrome formation and accompanied bimodal volcanic rocks occurring in the Baiyanggou area, south of Bogda Shan. The main lithotectonic units consist of olistostrome, volcanic rocks and turbidite. The olistostrome is tectonically underlain by Upper Carboniferous limestone and sandstone along a NEE-trending detachment fault. Paleo-growth fault is locally observed. The olistostrome unit includes plenty of blocks of limestone, sandstone, rhyolite and volcaniclastic rocks, and a matrix of greywacke. Limestone blocks are dated as Pennsylvanian-Bashkirian in age by the coral and brachiopod fossils that are extensively recognized in the Upper Carboniferous strata. The volcanic unit consists of pillowed and massive basalt and rhyolite, the latter occur as an 8-10-meter thick layer above the olistostrome unit. The turbidite unit is mainly composed of chert, siliceous mudstone and sandstone, within which the Bouma sequence can be locally recognized. Meter-wide gabbro and diabase dykes intrude these three units.

Geochemically, rhyolites are characterized by high ACNK value of >1.1, depletion of Ba, Nb and Sm, and enrichment in Rb, Th and Zr. Basaltic rocks are rich in K_2O, they show a LREE-enriched pattern and depletion in Ba, Nb and Zr, and enrichment in Ti, Ce and Hf, similar to continental rift-type tholeiite series. A gabbro porphyrite intruding the olistostrome was dated at 288 ± 3 Ma by a sensitive high-resolution ion microprobe (SHRIMP) zircon U-Pb method, and a rhyolite at 297 ± 2 Ma by a laser ablation inductively coupled plasma mass spectrometer (LA-ICPMS) zircon U-Pb method.

The Baiyanggou olistostrome and accompanying bimodal volcanic series are linked to an extensional setting that developed in the south of the Bogda Shan. Several lines of evidence, e.g. occurrence of large scale strike-slip shear zones, large number of mantle-derived magmatic rocks and available geochronological data, demonstrate a significant geodynamic change from convergence to extension in the Chinese Tianshan belt, even in the whole Central Asian Orogenic Belt. The extension in the Chinese Tianshan belt is initiated at ca. 300 Ma, i.e. around Carboniferous-Permian boundary times, and the peak period of intra-plate magmatism occurred in the interval of 300-250 Ma.

Key words: olistostrome; bimodal volcanic rocks; zircon U-Pb dating; Early Permian; Bogda Shan; Tianshan; Central Asian Orogenic Belt

Introduction

The Tianshan belt, sub-E-W-extending over 3000 km from NW China to Kazakhstan and Kyrgyzstan, is the southern part of the Central Asian Orogenic Belt (CAOB in short) and therefore important for understanding the geology of Central Asia. The CAOB was formed by amalgmation of various continental blocks, arc complex and accretionary wedges, and underwent subsequent polyphase tectonic evolution (Coleman 1989; Li et al. 2000, 2003; Zhao XX et al. 1990; Shu et al. 2003a; Windley et al. 1990, 2007; Xiao et al. 2008). The terrane amalgamation and related lithospheric shortening occurred in the Late Paleozoic (Allen et al. 1993, 1995, 2001; Li et al.; 2003, 2006a; Shu et al. 1997, 2000, 2002, 2003b; Laurent-Charvet et al. 2002, 2003; Jahn et al. 2004; Xiao et al. 2004a; de Jong et al. 2009; Wang et al. 2006, 2008, 2010; Charvet et al. 2007), forming a primary framework of the Tianshan orogenic belt. Two angular unconformities occurring in the pre-Permian strata documented the main orogenic events. The first one occurs between Early Carboniferous (Visean) conglomerate and Silurian schist in the Central Tianshan area; the second between Permian conglomerative bed and Carboniferous strata in the whole Tianshan belt (Guo et al. 2002; Xiao et al. 2004b; Charvet et al. 2007).

In the Kelamaili suture zone located in the east of Junggar block, Famennian-Tournaisian radiolarians were found in the chert of an ophiolitic suite (Shu and Wang 2003), and thus the latest Devonian-earliest Carboniferous age represents a lower limit of oceanic closure. In the Bayingou area, south of Junggar block, the Sikeshu granite intruding the ophiolitic mélange yielded SHRIMP zircon U-Pb age of 316 ± 3 Ma (Han et al. 2010). In Central Tianshan, the granite intruding the arc volcanic rocks was dated at 318 ± 5 Ma by SHRIMP zircon U-Pb method (Sun et al. 2006). These dates defined a crucial upper age constraint for the time of collision between terranes.

Previous works show that a post-collisional tectonic-magmatic event occurred in Chinese Tianshan belt since Early Permian (Shu et al. 2005; Charvet et al. 2007; de Jong et al. 2009; Wang et al. 2009). It is characterized mainly by large-scale strike-slip shearing and rifting as well as bimodal magmatism. Three large-scale Permian strike-slip ductile shear zones, sub-E-W-extending more than 600 km, developed in the Tianshan and Junggar areas. To the north, the Erqishi sinistral strike-slip shear zone is located in the southern margin of the Altai orogenic belt; to the south, the Main Tianshan Shear Zone or the Weiya–Bingdaban zone is a dextral strike-slip fault; and the middle zone is named the Kangguer-Huangshan dextral strike-slip shear zone (Shu et al., 2000). Bimodal volcanic rocks, consisting of alkaline basalt and rhyolite intercalated with clastic rocks, develop widely in the whole Tianshan belt. Alkaline granitic dykes and gabbro-diabase swarms intrude the pre-Permian rocks. Geochronological results suggest that the strike-slip shearing took mainly place in the interval of 290-245 Ma (Shu et al. 1999; Laurent-Charvet et al. 2003; de Jong et al. 2009), and the extensional magmatism was dated at 300-250 Ma (Jiang et al. 1999; Sun et al. 2006; Wang et al. 2009; Chen and Shu 2010).

The sub-E-W-trending Bogda Shan is an important tectonic belt separating the Junggar Basin to the north from the Turpan-Hami Basin to the south (Fig. 1). It has been considered as (1) a Carboniferous volcanic arc (Ma et al. 1993, 1997; Laurent-Charvet et al. 2003), (2) an intracontinental rifting zone during the Carboniferous-Permian time (He et al. 1994; Gu et al. 2000), (3) a Carboniferous volcanic arc superimposed by an Early Permian rift (Shu et al. 2005), or (4) a part of mantle plume related large igneous province (Xia et al. 2004).

In the southern Bogda Shan, an olistostrome was found in the Baiyanggou area, 30 km to the southeast of Urumqi City. Based on its geometric and structural features, Shu et al. (2005) proposed that the formation of the Baiyanggou olistostrome was a result of a post-collisional event accompanied by Early Permian syntectonic plutonism and bimodal volcanism.

In order to better understand the geological environment of the Baiyanggou olistostrome and its tectonic significance, and put more precise age constraint on its formation, in this paper, we present

new detailed description of the olistostrome, geochemistry and isotopic ages of the magmatic rocks, and conclude that the extension-related bimodal magmatism and olistostrome formation started around Carboniferous-Permian boundary times, thus marking the end of compressional tectonism in the North Tianshan.

Geological background

Structural outline

The Central part of Bogda Shan is mainly composed of Carboniferous sedimentary, volcanic and volcaniclastic rocks. These sequences were folded into an asymmetric anticline and subsequently cut by a detachment fault (Fig. 2). A gabbroic pluton of about 180 square kilometers intrudes the Carboniferous rocks. The gabbro is not directly dated, although a diabase dyke in the southern Bogda Shan was dated at 294 ± 1 Ma (Sm-Nd isochron) (Gu et al. 2001). The northern and southern slopes of the Bogda Shan are occupied by Permian sedimentary rocks that are intercalated with bimodal volcanic rocks in the southern slope.

Early Permian bimodal volcanic rocks occur in an E-W-extending zone of over 500 km-long in the southern foot of Bogda Shan (Fig. 1). This zone is also called the Shanshan-Qijiaojing-Kulai rift zone (Shu et al. 2005). The volcanic rocks are mainly composed of purple-colored ignimbrite, rhyolite and green-black basalt. The total thickness of bimodal volcanic series varies in different segments, but the basaltic rocks are usually thicker than rhyolitic rocks. Their ages remain undated although they have been assigned as Early Permian in the available geological map (scale 1/1,500,000) (XJBGMR 1992).

Several NE- to E-W-trending normal faults are widely developed in the studied area. Therein a detachment fault between Carboniferous and Permian sequences is considered as the boundary of the Early Permian rifting basin (Shu et al. 2005). Growth fault can be locally distinguished along the detachment fault according to the variation of the rocks thickness. The formation of detachment fault is assumed as earliest Permian since the fault cut Upper Carboniferous rocks, and the fault

plane was in turn cross-cut by an Early Permian gabbro dyke (cf. below) and also sealed by Permian sedimentary rocks (Fig. 2).

Triassic clastic rocks were thrust onto the Jurassic coal-bearing strata due to Cenozoic intracontinental events. All pre-Paleogene rocks were cut and displaced by Cenozoic thrust faults with a strike of NE or sub-E-W (Fig. 2). Most Paleozoic ductile thrust and strike-slip faults dated in the neighboring areas at the interval of Late Carboniferous to Permian (Ma et al. 1997; Shu et al. 2002; Laurent-Charvet et al. 2003) have been displaced or replaced by Cenozoic faults.

Stratigraphic sequences

According to drill-hole data (XJBGMR 1993), the Carboniferous-Permian sedimentary sequences develop upon the Silurian-Devonian metamorphic basement. The Carboniferous strata with a thickness of 1200-1800 m are the oldest rocks exposed in the Bogda Shan. It is divided into three formations, namely: the Lower Carboniferous Liushugou Formation (C_1l), Qijiagou Formation (C_1q), and Upper Carboniferous Aoertu Formation (C_2a) (XJBGMR 1960). These formations mainly consist of sandstone, mudstone, limestone, bioclastic limestone, tuff, basaltic rocks and andesite intercalated with rhyolite; the only difference is the fossil assemblages developed in these rocks.

The Permian strata, more than 3000 m thick, can be divided into three series. The Lower Permian defined as Jijicao Group (P_1jj) is composed of terrestrial coarse sandstone, sandstone, siltstone and neritic-bathyal facies turbitite, siliceous mudstone and chert intercalated with bimodal volcanic rocks or alkaline basalt. The Middle Permian is further subdivided into three formations (namely, Wulabo, Jingjingzigou, Lucaogou Formations) that are composed of terrestrial clastic rocks including purple conglomerate, coarse sandstone and greywacke and sandstone. The Upper Permian Hongyanci Formation is composed of lacustrine siltstone and mudstone.

The Middle Permian Wulabo Formation (purple conglomerate and coarse-grained sandstone) overlies unconformably the Lower Permian Jijicao Group, and then grades upwards into rhythmic

sandstone and mudstone of Jingjingzigou, Lucaogou and Hongyanci Formations.

Litho-tectonic units

The Baiyanggou olistostrome and associated rocks are exposed more than 20 km long and 3-5 km wide in the southwest of the Bogda Shan (Figs. 1, 2). Our field survey was conducted between N43°40'33", E88°03'21" and N43°42'13", E88°02'55". The outcrop is continuous forming a N-S trending section of ca. 2700 m long. Bedding dips to the south for ca. 60°. Three distinct lithotectonic units can be recognized, namely, an olistostrome unit containing intercalated basalt and rhyolite, a basalt unit and a turbidite unit (Fig. 3).

Olistostrome unit

This unit is ~1360 m wide at surface and can be divided into two parts. The lower part, with a width of 1200 m, consists of allochthonous blocks of limestone, sandstone and chert as well as volcanic breccia, which are surrounded by medium to fine-grained matrix of mudstone and tuff. Majority of blocks is grey-white limestone that occupies 60-70% of total content. The upper part of this unit is composed of greywacke with a thickness of 160 m, containing a small amount of irregular conglomerates of the underlying strata such as limestone and tuff. A bimodal volcanic series with a thickness of 8-10 m is intercalated in greywacke, consisting of fine-grained basalt and rhyolite. Microscopically, the rhyolite consists mainly of angular rock fragments (chert and sandstone), plagioclase-quartz crystal fragments and plastic glass with multi-angular camber and flame-like shapes.

Single olistolith exhibits various shape such as lens, breccia and sub-round with different sizes (Fig. 4C). The bigger blocks are limestone with sizes ranging from 100 m to 300 m in diameter, which includes brachiopoda and coral fossils; the brachiopoda was identified as *Choristites sp.* with a Late Pennsylvanian age, and the coral fossils are unclear in age due to extensive recrystallization (examination at Nanjing Institute of Geology and Palaeontology, Chinese Academy of Sciences,

unpublished data). The petrography and included fossils resemble those of the limestone of the Late Carboniferous Aoertu Formation in the Bogda area.

In the bottom of the olistostrome unit, a N70°E-trending main detachment fault zone, 15 m wide and dipping to the south at 65°, contacts with Late Carboniferous limestone and sandstone of the Aoertu Formation (Fig. 4A). An 80 cm wide gabbro dyke (Fig. 4E) dated at 288 Ma (cf. below) crosscuts the main detachment fault and olistostrome body, indicating that this main detachment fault was formed before 288 Ma. Growth fault and syn-sedimentary texture, such as convolute bedding and small sliding folds, can be observed in the lower part of this unit.

Near the main detachment fault, olistostrome formation was involved in south-verging asymmetric folds, in which cleavage occurs parallel to the south-dipping fold axial plane. Some small blocks of limestone and sandstone distribute preferentially in a NE50°-60° direction. Within or near the fault zone, breccia fragments of different size can be recognized. Two groups of joints in the contact zone were measured; their average directions are calculated from 115 measurements at 20°∠70° (dip/dip angle) and 80°∠72° (inset A of Fig. 3) and for 200°∠65° and 270°∠72° (inset B of Fig. 3). The drag folds and sheared cleavages are also common; acute angles between the axis of drag fold or cleavage and the main fault plane indicate a southeastward slipping of the hanging wall.

Basalt unit

This unit, 330 m wide (i.e., ~280 m thick), is divided into two parts. The lower part is 250 m wide and consists of pillow basalt; the 80 m-wide upper part is composed of massive basalt. The pillow basalts occur above the underlying olistostrome; and the massive basalts were intruded by a 30-50 cm wide dyke of diabase porphyrite. This unit is overlain by turbidite unit (cf. below).

Pillow basalt shows a typical hemispherical shape (Fig. 4D) demonstrating a sequence younger towards the SE of the section (Fig. 3). The crust of the pillow is composed of 2-3 cm thick chalcedony, and gaps among pillows are filled by glassiness and siliceous clay. The pillow bodies

have different sizes, the largest is up to 80 cm in diameter, the smallest is 10 cm and most pillows are 40-50 cm in diameter.

A vesicular structure is commonly observed in the pillow basalt. All vesicles are filled by amygdaloid calcite or quartz. The vesicular pillow basalt with porphyritic structure consists of phenocrysts of labradorite (An=65-70, 15 %), pyroxene (5-10 %), olivine (2-3 %) and groundmass composed of micro-crystals of plagioclase, pyroxene and chlorite (70%), as well as accessory minerals (magnetite+spinel, 2-4 %). Hornblende is also found to be associated with pyroxene phenocrysts. Most mafic micro-crystals in the groundmass have been replaced by chlorite.

Upward, the pillow lava becomes gradually massive basalt, in which vesicular structure can not be observed. Pillowed and massive basalts exhibit fracture and joint but not fold due to their rigid and massive physical property.

Turbidite unit

This unit, with a thickness of ~1100 m, overlies conformably the basalt unit. The top of this unit cannot be seen due to being covered by Quaternary alluvium. The turbidite unit is also divided into two parts: the lower part consists of grey turbidite sequence consisting of conglomerate-sandstone-siltstone-siliceous mudstone sequence (Fig. 4F), having a thickness of 350 m; the upper part, 750 m thick, is composed of grey-green laminar sandstone and massive mudstone.

A few decimeter-scale limestone blocks were observed in this unit. Rhythmic, graded and massive bedding, and small-scale growth fault (140∠60) are well developed. The graded bedding shows a normal sequence younger to the south. Layer-slip faults parallel to steep bedding-planes occur widely between above-mentioned three units, implying an extension after the olistostrome accumulation.

Geochemical features of igneous rocks

In order to determine the magma composition and understand the tectonic settings of the aforementioned volcanic rocks, 12 representative samples (5 basalts, 3 rhyolites, 1 gabbro and 3 diabases) were analyzed for major, trace and rare earth elements. Petrographic features of the samples are presented in Table 1. The sampling locations are shown on the cross-section (Fig. 3).

The major element contents were analyzed using XFR method by Zhang Mengqun in the Modern Analysis Center of Nanjing University, and the contents of rare earth and trace elements were determined by Gao Jianfeng using Finnigan MAT Element II-type ICP-MS in the State Key Laboratory for Mineral Deposits Research, Nanjing University. Analytical procedures are same as described by Rickwood (1989), Falkner et al. (1995) and Qi et al. (2000a, 2000b). Uncertainties for major elements represent 2% errors (XFR) and 5% for rare earth and trace elements (ICP-MS). REEs were normalized to chondrite values according to Sun and McDonough (1989), and trace elements to primitive mantle values following McDonough and Sun (1995).

All samples used for analysis are not-fractured and least altered. The loss on ignition (LOI) is usually low (0.34 to 1.55 wt %) except for the pillow basalt sample 2965 (2.35 %). Analytical results are shown in Table 2.

The Geochemical data show that the analyzed igneous rocks from the Baiyanggou section consist of basaltic and rhyolitic rocks. Five basaltic samples show similar features, they have high content of SiO_2 (51.4-52.7 %) that could have been elevated by input of secondary quartz amygdales. They are richer in Na_2O (2.78-3.81 %) than in K_2O (~0.90 %). They show LREE-enriched patterns (La_N/Yb_N = 5.3-7.4), with weak negative or no significant Eu anomalies (Eu/Eu* = 0.79-1.03) (Fig. 5A; Table 2). In the trace element spider-diagrams (Fig. 5B), enrichment of Ti, Ce, Hf and depletion of Ba, Nb, Zr can be observed, these features are similar to those of continental rift-type basalt (Condie 1989; Wilson 1989; Furman 2007). The gabbro and diabase porphyrite show similar geochemical characteristics in REEs and trace elements to the basalts (Figs. 5A, B).

Compared with the basaltic rocks, three rhyolitic samples are poorer in plagioclase and biotite, and richer in potassic feldspar and sanidine. In major element compositions, all rhyolitic samples

are K-riched, with high total alkalies (K_2O+Na_2O) contents of 7.11-9.08 %. They are poor in CaO and MgO contents (Table 2). Their ANKC values (Mol Al_2O_3 / (Na_2O+K_2O+CaO)) are 0.86-0.94.

All rhyolitic samples have high total contents of rare earth elements of 198-207 ppm. They show LREE-enriched patterns, with significant negative Eu anomalies (Eu/Eu* = 0.22-0.39) (Fig. 5C; Table 2), suggesting a marked fractionation between LREE and HREE. Their primitive-mantle-normalized trace element patterns show prominent enrichment of Rb, Th, Zr and Hf (Fig. 5D). These features are comparable to the rift-related rhyolitic rocks (Li et al. 2008). A distinct negative Nb anomaly can be observed. This feature could be related to a mantle source modified by subduction related material as observed in post-collisional magmatic rocks (Wang et al. 2009; de Jong et al., 2009).

In the Nd*2-Zr/4-Y and Ti versus Zr discrimination diagrams, most of samples plot either in the within-plate tholeiite field (Fig. 6A) or in the within-plate basalt field (Fig. 6B).

Zircon U-Pb dating of igneous rocks

Sampling and analytical techniques

In order to constrain the age of olistostrome in the Baiyanggou area, we conducted SHRIMP and LA-ICPMS U-Pb dating on the zircons from the igneous rocks. One gabbro (Sample 234) was collected from the lower part of olistostrome unit (Fig. 3). Sample 2891 was collected from rhyolite layer located above the olistostrome (Table 1; Fig. 3).

Zircon grains were hand-picked from the crushed sample power after heavy liquids and magnetic separation. Most zircon grains are light purple, transparent and idiomorphic-hypidiomorphic. Zircon grains from the gabbro are smaller (20-50 μm in diameter) than those from the rhyolite (ca. 40-80 μm). Zircon mounting, microscopic and cathodo-luminescence (CL) photography were performed in the Center of Ion-Probe in Beijing.

The zircons of gabbro were analyzed using a SHRIMP II, the beam size is 30 μm. Standard zircons (TEM) from Australia were used for correction of isotopic fractional distillation and

determination of U, Th, Pb contents. Common Pb was corrected with measured ^{204}Pb of standard (TEM). Detailed analytical procedures have been described by Compston et al. (1984, 1992) and Kröner et al. (1998). The data were analyzed with Ludwig's SQUID 1.02 and ISOPLOT 2.06 (Ludwig 1999).

Age dating of the zircons from Sample 2891 from the upper part of olistsotrome unit was carried out at the State Key Laboratory for Mineral Deposits Research (Nanjing University), using the Agilent 7500s ICPMS coupled with a New Wave 213 μm laser ablation (LA) system with an in-house sample cell. Detailed analytical procedures are similar to those described by Griffin et al. (2004), Jackson et al. (2004) and Wang XL et al. (2007). In order to control instrument stability and analytical accuracy, two analyses of the GJ zircon standard (608 ± 1.5 Ma; Jackson et al. 2004) and one analysis of standard MudTank (732 ± 5 Ma; Black and Gulson 1978) were done after each 10 analyses of zircon samples. All analyses were carried out using a beam width of 40 μm. U–Pb ages were calculated from the raw signal data using on-line software package GLITTER (ver. 4.4) (http://www.mq.edu.au/GEMOC). Common lead was corrected using the EXCEL-embedded program ComPbCorr#3 15G by Andersen (2002).

All errors are quoted in 1 sigma level, and weighted mean apparent ages were then calculated in 2 sigma level with 95% confidence.

Results and age significance

Twelve zircon grains of gabbro porphyrite (Sample 234) were analyzed. The analytical results are presented in Table 3. Most analytical data are concordant (Fig. 7A). Eight analyses yielded apparent $^{206}Pb/^{238}U$ ages ranging from 276~300 Ma, a mean age was calculated at 287.5 ± 3.4 Ma, which is interpreted as the crystallization age of the gabbro. Three analyses with older apparent $^{206}Pb/^{238}U$ ages of 315-323 Ma gave a mean age of 320.8 ± 4.2 Ma. This age is significantly older, and is therefore considered as the inherited zircons from the Carboniferous arc-type magmatic rocks. The rest one analysis yielded a much older age of 1826 ± 10 Ma (Table 3) that is probably derived from

a Paleoproterozoic basement rock in the deep crust of the studied area, but could also be a result of contamination.

Twenty-four zircon grains of rhyolitic sample 2891 were analyzed using the Laser Ablation Inductively Coupled Plasma-Mass Spectrometry (LA-ICP-MS) method. The dating results are listed in Table 4. All dated zircons show a clear zoning, and have Th/U ratios of 0.25-0.63 (average 0.40). Most ages are consistent within errors and accordant except analyses 1, 8 and 23 (Fig. 7B) that are not involved in mean age calculation. The other 21 analyses yielded a mean $^{206}Pb/^{238}U$ age of 296.6 ± 1.8 Ma with a MSWD value of 0.05.

This age is a little older than that of gabbro (288 ± 3 Ma), in agreement with the field occurrence of intrusive contact between the gabbro dyke and rhyolite. Thus, the ages of 297-288 Ma are the peak period of building the Baiyanggou olistostrome formation and companied bimodal magmatism.

Relationship with the Late Paleozoic tectonic events in the southern margin of CAOB

During the Paleozoic, three continental plates, namely, Tarim, Kazakhstan and Siberia, as well as small blocks with various affinities (arc, seamount, continental crust and oceanic crust) such as Altai, Dalbut, Junggar, Central Tianshan and Yili-North Tianshan occupied the Central Asia. Since Late Devonian, Kazakhstan Ocean (also called Tianshan-Mongolian Ocean in some literatures) subducted southward beneath the Tarim plate, producing the Bogda and Yili-North Tianshan volcanic arcs, and a block-amalgamation took subsequently place. This event affected strongly the southern margin of the CAOB, leading to the accretion of terranes (Xiao XC et al. 1990; Sengör et al. 1993; Shu et al. 2002, 2004; Wang et al. 2006, 2007a, 2008; Charvet et al. 2007; Windley et al. 2007; Xiao et al. 2004a, 2004b, 2008). Ophiolites, glaucophane-schist-bearing mélanges, mylonitic rocks and I-type granitoids were formed in response to such geodynamic processes (Windley et al. 1990, 2007; Allen et al. 1993, 1995; Gao et al. 1998; Jahn et al. 2004; Li et al. 2006a, 2006b;

Abrajevitch et al. 2008; Wang et al. 2010). The aforementioned SHRIMP zircon U-Pb age of 321 ± 4 Ma from the inherited zircons captured by the Baiyanggou gabbro dyke is interpreted as the timing of arc-related magmatism of the Bogda Shan.

Reconstruction of the Xinjiang paleogeography suggests that the marine environment of Tianshan-Junggar domain was gradually reduced both in surface and depth during the Carboniferous time (XJBMR 1993), and the peak of marine consumption took place in the Late Carboniferous (Zhou and Dean 1996).

The ophiolitic mélange, mylonite and amphibole-bearing granites are distributed along the different suture zones, which were sealed by a regional unconformity of Middle-Late Permian coarse sediments, providing an upper limit of suturing time (Gao et al. 1998; Shu et al. 2000, 2001; Charvet et al. 2007; Wang et al. 2007a). The siliceous rocks of ophiolite suite were dated at the Famennian-Tournaisian by radiolarian fossils (Shu and Wang 2003; Shu et al. 2007; Liu et al. 2006), representing the lower limit of suturing time. This suturing built the Tianshan range and various deformation structures such as folding and thrust-stacking.

Since Early Permian or late stage of Late Carboniferous, the termination of oceanic subduction and subsequently slab detachment caused lithospheric thinning, upwelling of mafic magma and strike-slip shearing that is widespread in the southern margin of CAOB including Chinese Tianshan belt (e.g. de Jong et al., 2009; Wang et al. 2009). This event could be linked to an extensional event in the Chinese Tianshan belt and neighboring Kyrgystan and Kazakhstan orogenic belts (Natal'in and Sengör 2004; Charvet et al. 2007).

As aforesaid, in the Baiyanggou olistostrome domain, the bimodal volcanic rocks, pillow basalts and alkaline gabbro/diabase dykes of 288 Ma were derived from mantle magma with partly contribution of crustal material. Geochemically, these rocks show an affinity of rifting setting. We assume that the gabbros/diabases in the central part of the Bogda Shan were probably generated in a similar environment although their geochronological and geochemical features still need to be further studied.

Thus, with more and more multidisciplinary data obtained, the previous tectonic interpretations of the study area should be re-evaluated. Firstly, a Late Paleozoic passive margin (e.g. He et al. 1994) is no longer supported by newly published data since the study area underwent a subduction-related convergent regime with production of magmatic arc system. Secondly, the hypothesis of mantle plume is considered unlikely due to lacking of basic geological evidence rather than geochemical significance (de Jong et al., 2009; Wang et al. 2009). Moreover, a Late Paleozoic volcanic arc should be also constrained more precisely, i.e., a Late Devonian-Carboniferous volcanic arc (e.g. Wang et al. 2007a) was followed by Permian extension and rift-related post-collisional magmatism.

It is worth emphasizing that the Baiyanggou olistostrome-bearing sequence records a deepening sedimentary environment. The olistostrome series with the blocks of Late Carboniferous platform facies limestone and the matrix of greywacke (Unit 1) indicates a collapse likely linked to a post-collision setting. The pillow basaltic rocks (Unit 2) represent an underwater eruption, and a turbidite-chert assemblage with Bouma sequence (Unit 3) suggests a deep-water sedimentation. Thus, we conclude that a deep-water environment existed still in some localities in the southern margin of Chinese Tianshan area.

Recently, $^{40}Ar/^{39}Ar$ dating showed that the strike-slip shearing in Chinese Tianshan and Altai took mainly place in the interval of 290-245 Ma. The aforementioned Erqishi sinistral strike-slip zone was dated at 281 ± 8 Ma and 289 ± 4 Ma on muscovite of gneiss (Laurent-Charvet et al. 2002). The Main Tianshan Shear Zone or the Weiya–Bingdaban dextral shearing zone yield a muscovite age of 269 ± 5 Ma (Shu et al. 2002); the shearing of North Tianshan Fault occurring during 285-250 Ma (de Jong et al. 2009); ductile strike-slip faulting in Nalati Fault continued up to 260-250 Ma (Wang et al. 2007b); the ductile deformation of the Kangguer-Huangshan zone was dated around 260-247 Ma on muscovite (Wang YT et al. 2004) and 247 ± 1 Ma on biotite of mylonite (Chen W et al. 2004). These regional strike-slip faults are correlated both in space and in time with the Permian extensional structure and magmatism, and can be therefore considered to be linked to be

response of collisional (Shu et al. 2005) or oblique-collisional tectonics (de Jong et al., 2009; Wang et al. 2009). This link between the post-collisional transcurrent tectonics and synchronous magmatism and metallogeny is a common feature of Central Asian Orogenic Belt in Late Paleozoic times (de Jong et al., 2009; Pirajno 2010).

As reported by previous researchers, mafic dykes and alkaline rocks dated as Permian are widely distributed in the Tarim block and its surrounding ogogenic belts (Chen HL et al. 1997; Jiang et al. 1999; Wang JB et al. 2006; Zhang et al. 2008), showing a violent magmatism under an extensional setting. As seen in the Kuruqtag segment of the NE-Tarim block and the central and southern Tianshan belt, the interbedded diabase and granite dykes with a bimodal geochemical feature construct a marked ―zebra mountain sight (Figs. 8A, B). The dating values of bimodal igneous series or alkaline basalts are concentrated in the interval of 300-250 Ma (Zhao ZH et al. 2000; Chen HL et al. 1997; Shu et al. 2005; Li et al. 2006b; Wang B et al. 2009).

Furthermore, the Baiyanggou olistostrome yielded two isotopic ages, 288 ± 3 Ma (SHRIMP U-Pb) on the gabbro dyke and 297 ± 2 Ma (LA-ICPMS U-Pb) on the rhyolite, respectively, consistent with the dating of the neighboring Karlik granites of 297 ± 2 Ma and 295 ± 2 Ma (LA-ICP-MS zircon U-Pb) (Chen and Shu 2009), representing a likely initial time of extensional event.

As observed in the Baiyanggou section, a local marine basin existed during Early Permian while coeval strike-slip shearing and extensional magmatism as well as olistostrome were developed in the Tianshan belt. The Early Permian turbidite-chert sequence and pillow lava in the Baiyanggou area confirm this conclusion. Since Middle-Late Permian, paleo-Tianshan ocean was entirely closed, a regional-scale Middle-Late Permian unconformity accompanied with a thick molasse sequence indicate the termination of a marine setting and the beginning of a welded terrestrial environment for the Tianshan area of the CAOB.

Conclusions

An olistostrome formation occurs in the south of the Bogda Shan, it is overlain by bimodal

volcanic rocks and turbidite sequence, and intruded by gabbro and diabase dykes. Geochemical analyses on the volcanic rocks suggest that they formed in an intraplate setting with contribution of subduction-related magma source. Olistoliths include blocks of Late Carboniferous limestone. Zircon SHRIMP and LA-ICPMS dating on the overlying rhyolite and intruding gabbro gyke yielded ages of 297 and 288 Ma, respectively. These stratigraphic and chronological data constrain the timing of the olistostrome at the Carboniferous-Permian boundary. Occurrences of normal fault, regional large-scale strike-slip shear zones and coeval magmatism suggest an extensional setting that developed in the south of the Bogda Shan. The extension in the Chinese Tianshan belt is initiated at ca. 300 Ma, and laterally comparable throughout in the Central Asian Orogenic Belt.

Acknowledgements

The authors are grateful to Profs. Sun S, Jahn B M and Xiao W J for their enthusiastic helps and fruitful advising on this study. We thank Prof. K. de Jong and one anonymous reviewer for their constructive comments and suggestions that are very helpful for improving our paper. We wish to express our thanks to Profs. Liu Dunyi, Song Biao, Jian Ping, Wan Yusheng and Tao Hua of Center of Iron-Probe in Beijing and Dr. Wang Xiaolei of Nanjing University for their guides during SHRIMP and LA-ICPMS U-Pb dating. Profs. Ma Yingjun and Wang Baolin are thanked for their supports in field work. Dr. Davis H, who is teaching in the Department of Applied Foreign Language Studies of the Nanjing University, is thanked for his help in improving English. This study was sponsored by the National Basic Research Program of China (973 Program, No. 2007CB411301) and the State Key Laboratory for Mineral Deposits Research (Nanjing University) (No. 2008-I-01).

References

Abrajevitch A, Van der Voo R, Bazhenov ML (2008) The role of the Kazakhstant orocline in the late Paleozoic amalgamation of Eurasia. Tectonophysics 455: 61-76

Allen MB, Windley BF, Zhang C (1993) Paleozoic collisional tectonics and magmatism of the Chinese Tien Shan, central Asia. Tectonophysics 220: 89-115

Allen MB, Sengor AMC, Natal'in BA (1995) Junggar, Turfan, and Alakil basins as Late Permian sinistral pull-apart structures in the Altaid orogenic collage, central Asia. J Geol Soc Lond 152: 327-338

Allen MB, Alsop GI, Zhemchuzhnikov VG (2001) Dome and basin refolding and transpressive inversion along the Karatau fault system, southern Kazakstan. J Geol Soc Lond 158: 83-95

Andersen T (2002) Correction of common Pb in U–Pb analyses that do not report ^{204}Pb. Chem Geol 192: 59–79

Black LP, Gulson BL (1978) The age of the Mud Tank carbonatite, Strangways Range, Northern Territory. BMR J Aust Geol Geophys 3: 227–232

Charvet J, Shu LS, Laurent-Charvet S (2007) Paleozoic structural and geodynamic evolution of eastern Tianshan (NW China): welding of the Tarim and Junggar plates. Episodes 30: 162-186

Chen HL, Yang SF, Dong CW, Jia CZ, Wei GQ, Wang ZG (1997) Confirmation of Permian basite zone in Tarim Basin and its tectonic significance. Geochimica 26: 77-87

Chen W, Wang YT, Zhang Y, Han CM (2004) Study on the genesis of Kanggur gold deposit, NW China. Geochim Cosmochim Acta Suppl 68: A627

Chen XJ, Shu LS (2010) Features of the post-collisional tectono-magmatism and geochronological evidence in the Karlik Mt., Xinjiang. Acta Petrol Sin, in press

Coleman RG (1989) Continental growth of northwest China. Tectonics 8: 621-635

Compston W, Williams IS, Meyer C (1984) U-Pb geochronology of zircons from lunar breccia 73217 using a sensitive high mass resolution microprobe. J Geophys Res 89 (Suppl): B325-534

Compston W, Williams IS, Kirchvink JL (1992) Zircon U-Pb ages for the Early Cambrian time

scale. J Geol Soc Lond 149:171-184

Condie KC (1989) Plate tectonics and crustal evolution. Pergamon Press, Oxford, p. 476

de Jong K, Wang B, Faure M, Shu LS, Cluzel D, Charvet J, Ruffet G, Chen Y (2009) New 40Ar/39Ar age constraints on the Late Palaeozoic tectonic evolution of the western Tianshan (Xinjiang, northwestern China), with emphasis on late Permian fluid ingress. Int J Earth Sci 98, 1239-1258

Falkner KK, Klinkhammer GP, Ungerer CA, Christie DM (1995) Inductively coupled plasma mass spectrometry in geochemistry. Annu Rev Earth Planet Sci 23: 409 - 449

Pirajno F (2010) Intracontinental strike-slip faults, associated magmatism, mineral systems and mantle dynamics; examples from NW China and Altay-Sayan (Siberia). J Geodynam doi:10.1016/j.jog.2010.01.018

Furman T (2007) Geochemistry of East African Rift basalts: An overview. J Afri Earth Sci 48: 147-160

He GQ, Li MS, Liu DQ, Zhou RH (1994) Paleozoic crustal evolution and mineralization in Xinjiang of China. Xinjiang People's Publ House, Urumqi, p. 437 (in Chinese with English abstract)

Hu AQ, Zhang GX, Zhang QF, Chen YB (1999) Constraints on the age of basement and crustal growth in Tianshan Orogen by Nd isotopic composition. Sci Chin (D) 20:104-112 (in Chinese)

Gao J, Li MS, Xiao XC, Tang YQ, He GQ (1998) Paleozoic tectonic evolution of the Tianshan Orogen, northwestern China. Tectonophysics 287: 213-231

Griffin WL, Belousova EA, Shee SR, Pearson NJ, O'Reilly SY (2004) Archean crustal evolution in the northern Yilgarn Craton: U–Pb and Hf-isotope evidence from detrital zircons. Precambrian Res 131: 231–282

Gu LX, Yu CS, Hu SX, Li HY (2000) Carboniferous volcanites in the Bogda orogenic belt of eastern Tienshan: their tectonic implications. Acta Petrol Sin 16: 305-316 (in Chinese with

English abstract)

Gu LX, Hu SX, YU CS, Zhao M, Wu CZ, Li HY (2001) Intrusive activities during compression-extension tectonic conversion in the Bogdaintracontinental orogen. Acta Petrol Sin 17: 187-198 (in Chinese with English abstract)

Guo J, Shu LS, Charvet J, Laurent-Charvet S, Sun SW (2002) Geochemical features of the two Early Paleozoic ophiolitic zones and the volcanic rocks in the Central-Southern Tianshan region, Xinjiang. Chin J Geochem 21: 308-321

Jackson SE, Pearson NJ, Griffin WL, Belousova EA (2004) The application of laser ablation-inductively coupled plasma-mass spectrometry to in situ U–Pb zircon geochronology. Chem Geol 211: 47–69

Jahn BM, Wu FY, Chen B (2000) Granitoids of the Central Asian Orogenic Belt and continental growth in the Phanerozoic. Transact Roy Soc Edinburgh: Earth Sci 91: 181–193

Jahn BM, Windley B, Natal'in B, Dobretsov N (2004) Preface -Phanerozoic continental growth in Central Asia. Preface. J Asian Earth Sci 23: 599-603

Jiang CY, Mu YM, Bai KY, Zhao XN, Zhang HB, Hei AZ (1999) Chronology, petrology, geochemistry and tectonic environment of granitoids in the southern Tianshan Mountain, western China. Acta Petrol Sin 15: 298-308 (in Chinese with English abstract)

Kröner A, Cui WY, Wang SQ, Wang CQ, Nemchin AA (1998) Single zircon ages from high-grade rocks of the Jianping Complex, Liaoning Province, NE China. J Asian Earth Sci 16: 519–532

Laurent-Charvet ., Charve, ., Shu, LS, Ma RS, Lu HF (2002) Palaeozoic late collisional strike-slip deformations in Tianshan and Altay, Eastern Xinjiang, NW China. Terra Nova 14: 249-256

Laurent-Charvet S, Monié P, Charvet J, Shu LS, Ma RS (2003) Late-Paleozoic strike-slip shear zones in northeastern Xinjiang (NW China): new structural and geochronological data. Tectonics 22:1099-1101

Li JY, Xiao XC, Chen W (2000) Late Ordovician continental basement of the eastern Junggar basin in Xinjiang, NW China: Evidence from the Laojunmiao metamorphic complex on the

northeast basin margin. Region Geol Chin 19: 297-302 (in Chinese with English abstract)

Li JY, Xiao WJ, Wang KZ, Sun GH, Gao LM (2003) Neoproterozoic-Paleozoic tectonostratigraphy, magmatic activities and tectonic evolution of eastern Xinjiang, NW China. In: Mao JW, Goldfarb RJ, Seltmann R, Wang DH, Xiao WJ, Hart C (eds) Tectonic evolution and metallogeny of the Chinese Altay and Tianshan. Proceedings of the International Symposium of the IGCP-473 Project, IAGOD Guidebook Series 10, CERCAMS/NHM London, p.31-74

Li JY, He GQ, Xu X, Li HQ, Sun GH, Yang TN, Gao LM, Zhu ZX (2006a) Crustal tectonic framework of Northern Xinjiang and adjacent regions and its formation. Acta Geol Sin 80: 148-168 (in Chinese with English abstract)

Li JY, Wang KZ, Li YP, Sun GH, Chu CH, Li LQ, Zhu ZX (2006b) Geomorphological features, crustal composition and geological evolution of the Tianshan Mountains. Geol Bull Chin 25: 895-909 (in Chinese with English abstract)

Li WX, Li XH, Li ZX (2008) Middle Neoproterozoic syn-rifting volcanic rocks in Guangfeng, South China: petrogenesis and tectonic significance. Geol Mag 145(4): 475-489

Liegeois JP (1998) Preface—Some words on the post-collisional magmatism. Lithos 45: xv-xvii

Liu Y, Hao SG (2006) Evolutionary significance of Pylentonemid Radiolarians and their Late Devonian species from southwestern Tianshan, China. Acta Geol Sin 80: 647-655

Ludwig KR (1999) Isoplot/Ex version 2.06: A geochronological toolkit for Microsoft Excel. Berkeley Geochronology Center Special Publication, p. 48

Ma RS, Wang CY, Ye SF (1993) The outline of plate tectonics and crustal evolution in the eastern Tianshan belt, China. Nanjing Univ Publ House, Nanjing, p. 225 (in Chinese)

Ma RS, Shu LS, Sun JQ (1997) Tectonic evolution and metallization in the Eastern Tianshan belt, China. Geol Publ House, Beijing, p. 202 (in Chinese with English abstract)

McDonough WF, Sun SS (1995) The composition of the earth. Chem Geol 120: 223-253

Miller C, Schuster R, Klotzli U (1999) Post-collisional potassic and ultrapotassic magmatism in SW

Tibet: Geochemical and Sr-Nd-Pb-O isotopic constrains for mantle source characteristics and petrogenesis. J Petrol 40: 1399-1424

Natal'in BA, Sengör AMC (2004) Late Palaeozoic to Triassic evolution of the Turan and Scythian platforms: The pre-history of the Palaeo-Tethyan closure. Tectonophysics 404: 175-202

Pearce JA, Harris NBW, Tindle AG (1984) Trace element discrimination diagrams for the tectonic interpretation of granitic rocks. J Petrol 25: 956-983

Qi L, Gregoire DC (2000a) Determination of trace elements in twenty six Chinese geochemistry reference materials by inductively coupled plasma-mass spectrometry. Geostandards Newsletter 24: 51-63

Qi L, Gregoire DC (2000b) Determination of trace elements in granites by inductively coupled plasma-mass spectrometry. Talanta 51: 507-513

Rickwood PC (1989) Boundary lines within petrologic diagrams which use oxides of major and minor elements. Lithos 22: 247-263

Sengor AMC, Natal'in BA, Burtman B (1993) Evolution of the Altaid tectonic collage and Paleozoic crustal growth in Eurasia. Nature 364: 299-307

Shu LS, Ma RS, Wang CY (1997) Research on the thrust tectonics of the Eastern Tianshan belt, Xinjiang. Acta Geol Sin 32: 337-350 (in Chinese with English abstract)

Shu LS, Charvet J, Guo LZ, Lu HF, Laurent-Charvet S (1999) A large-scale Paleozoic dextral ductile strike-slip zone: the Aqqikkudug-Weiya zone along the northern margin of the Central Tianshan belt, Xinjiang, NW China. Acta Geol Sin 73: 43-81

Shu LS, Chen YT, Lu HF, Charvet J (2000) Paleozoic accretionary terranes in Northern Tianshan, NW China. Chin Geochem 19: 193-202

Shu LS, Lu HF, Yin DH, Ma RS, Charvet J, Laurent-Charvet S (2001) Late Paleozoic continental accretionary tectonics in Northern Xinjiang. Xinjiang Geol 19: 59-63 (in Chinese with English abstract)

Shu LS, Charvet J, Lu HF, Laurent-Charvet S (2002) Paleozoic accretion-collision events and

kinematics of ductile deformation in the eastern part of the southern-central Tianshan Belt, China. Acta Geol Sin 76: 308-323

Shu LS, Lu HF, Yin DH, Wang B (2003a) Paleozoic tectonic events and structural deformation in the Eastern Tianshan Belt, China. J Nanjing Univ (Natural Sci) 39: 17-30 (in Chinese with English abstract)

Shu LS, Wang B, Yang F, Lu HF, Charvet J, Laurent-Charvet S (2003b) Polyphase Tectonic events and Cenozoic basin-range coupling in the Tianshan belt, northwestern China. Acta Geol Sin 77: 457-467

Shu LS, Wang YJ (2003) Late Devonian-Early Carboniferous Radiolarian Fossils from Siliceous rocks of the Kelameili Ophiolite, Xinjiang. Geol Rev 49: 408-412 (in Chinese with English abstract)

Shu LS, Deng P, Wang B, Tan ZZ, Yu XQ, Sun Y (2004) Lithology, Kinematics and Geochronology Related to Late Mesozoic Basin-Mountain Evolution in the Nanxiong-Zhuguang Area, South China. Sci Chin (D) 47: 673-688

Shu LS, Wang B, Zhu WB (2007) The Age and Tectonic Significance of Radiolarian Fossils from the Heiyingshan Ophiolitic Mélange, Southern Tianshan Belt, NW China. Acta Geol Sin 81: 1161-1168 (in Chinese with English abstract)

Sun GH, Li JY, Yang TN, Wang Y, Gao LM, Hao SF (2006) Permian post-collisional N-S-compression deformation in Tianshan orogen: example from Koumenzi ductile shear zone of thrusting-type in northern slope of Karlik mountains. Acta Petrol Sin 22: 1359-1368 (in Chinese with English abstract)

Sun SS, McDonough WF (1989) Chemical and isotopic systematics of oceanic basalts: implications for mantle composition and Processes. In: Saunders AD, Norry MJ (eds) Magmatism in the ocean basins. Geol Soc Lond Spec Publ 42: 313-345

Van der Voo R, Levashova NM, Skrinnik LI (2006) Late orogenic, large-scale rotations in the Tien Shan and adjacent mobile belts in Kyrgystan and Kazakhstan. Tectonophysics 426: 335-360

Wang B, Faure M, Cluzel D, Shu LS, Charvert J, Ma Q (2006) Late Paleozoic tectonic evolution of the northern West Chinese Tianshan Belt. Geodinamica Acta 19: 237-247

Wang B, Shu LS, Cluzel D, Faure M, Charvet J (2007a) Geochemical constraints on Carboniferous volcanic rocks of Yili Block (Xinjiang, NW China); implications on tectonic evolution of Western Tianshan. J Asian Earth Sci 29: 148-159

Wang B, Shu LS, Faure M, Cluzel D, Charvet J (2007b) Paleozoic tectonism and magmatism of Kekesu-Qiongkushitai section in southwestern Chinese Tianshan and their constraints on the age of the orogeny. Acta Petrol Sin 23: 1354-1368 (in Chinese with English abstract)

Wang B, Cluzel D, Shu LS, Faure M, Charvet J, Chen Y, Meffre S, de Jong K (2009) Evolution of calc-alkaline to alkaline magmatism through Carboniferous convergence to Permian transcurrent tectonics, western Chinese Tianshan. Int J Earth Sci 98: 1275-1298

Wang B, Faure M, Shu LS, de Jong K, Charvet J, Cluzel D, Jahn BM, Chen Y, Ruffet G (2010) Structural and geochronological study of High-Pressure metamorphic rocks in the Kekesu section (Northwestern China): implications for the late Paleozoic tectonics of the southern Tainshan. J Geol 118: 59-77

Wang B, Faure M, Shu LS, Cluzel D, Charvet J, de Jong K, Chen Y (2008) Paleozoic geodynamic evolution of the Yili Block, Western Chinese Tianshan. Bulletin de la Société Géologique de France 179(5): 483-490

Wang JB, Xu X (2006) Post-collisional Tectonic Evolution and Metallogenesis in Northern Xinjiang, China. Acta Geol Sin 80: 23-31 (in Chinese with English abstract)

Wang T, Hong DW, Jahn BM, Tong Y, Wang YB, Han BF, Wang XX (2006) Timing, Petrogenesis, and Setting of Paleozoic Synorogenic Intrusions from the Altai Mountains, Northwest China: Implications for the Tectonic volution of an Accretionary Orogen. J Geol 114: 735–751

Wang XL, Zhou JC, Griffin WL, Wang RC, Qiu JS, O'Reilly SY, Xu XS, Liu XM, Zhang GL

(2007) Detrital zircon geochronology of Precambrian basement sequences in the Jiangnan orogen: dating the assembly of the Yangtze and Cathysia blocks. Precambrian Res 159: 117–131

Wang YT, Mao JW, Li XF, Yang FQ (2004) Gold metallization related to shear zone. Earth Sci Front 11: 393-400 (in Chinese with English abstract)

Wilson M (1989) Igneous Petrogenesis. London, Unwin Hyman, p. 466

Windley BF, Allen MB, Zhang C, Zhao ZY, Wang GR (1990) Paleozoic accretion and Cenozoic redeformation of the Chinese Tienshan range, Central Asia. Geology 18: 128-131

Windley BF, Alexeiev D, Xiao WJ, Kroner A, Badarch G (2007) Tectonic models for accretion of the Central Asian Orogenic Belt. J Geol Soc Lond 164: 31–47

Xia LQ, Xia ZC, Xu XY, Li XF, Ma ZP, Wang LS (2004) Carboniferous Tianshan igneous megaprovince and mantle plume. Geol Bull Chin 23: 903-910

Xiao XC, Tang YQ, Li JY, Zhao M, Feng YM, Zhu BQ (1990) On the tectonic evolution of the northern Xinjiang, Northwest China. Geosci Xinjiang 1: 47-68 (in Chinese with English abstract)

Xiao WJ, Windley BF, Badarch G, Sun S, Li JL, Qin KZ, Wang Z (2004a) Palaeozoic accretionary and convergent tectonics of the southern Altaids: implications for the growth of Central Asia. J Geol Soc Lond 161: 339-342

Xiao WJ, Zhang LC, Qin KZ, Sun S, Li JL (2004b) Paleozoic accretionary and collisional tectonics of the eastern Tianshan (China): implications for the continental growth of Central Asia. Am J Sci 304: 370–395

Xiao WJ, Han CM, Yuan C, Sun M, Lin SF, Chen HL, Li ZL, Li JL, Sun S (2008) Middle Cambrian to Permian subduction-related accretionary orogenesis of North Xinjiang, NW China: implications for the tectonic evolution of Central Asia. J Asian Earth Sci 32:102–117. doi:110.1016/j.jseas.2007.1010.1008

Xinjiang Bureau of Geology and Mineral Resources (XJBGMR) (1992) Geological map of Xinjiang Uygur Autonomy Region (scale1:1500000). Beijing, Geol Publ House (in Chinese)

Xinjiang Bureau of Geology and Mineral Resources (XJBGMR) (1993) Regional geology of Xinjiang Uygur Autonomy Region. Beijing, Geol Publ House, p. 841 (in Chinese with English abstract)

Zhang CL, Li XH, Li ZX, Ye HM, Li CN (2008) A Permian Layered Intrusive Complex in the Western Tarim Block, Northwestern China: Product of a Ca. 275-Ma Mantle Plume? J Geol 116: 269-287

Zhao XX, Coe RS, Zhou YX, Wu HR, Wang J (1990) New paleomagnetic results from northern China: collision and suturing with Siberia and Kazakhstan. Tectonophysics 181: 43-81

Zhao ZH, Bai ZH, Xiong XL, Mei HJ, Wang YX (2000) Geochemistry of alkali-rich igneous rocks of Northern Xinjiang and its implications for geodynamics. Acta Geol Sin 74: 321-328

Zhou ZY, Dean WT (1996) Phanerozoic geology of Northwest China. Beijing, Sci Press, p.251

Captions of figures

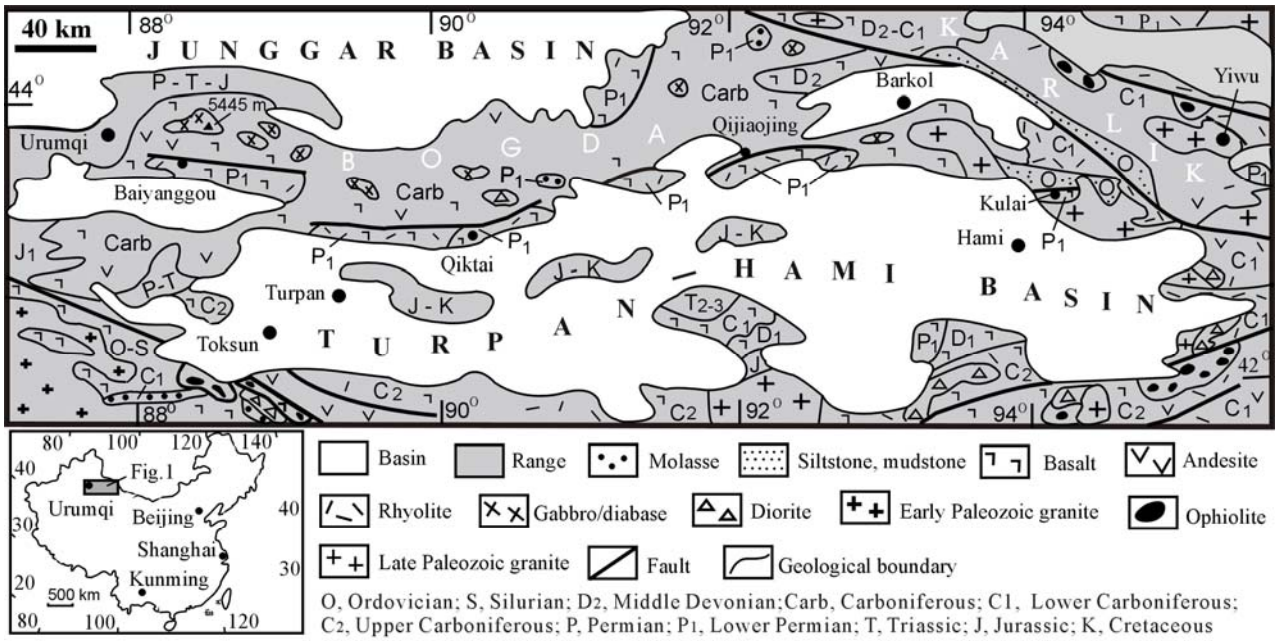

Figure 1. Simplified geological map of the Bogda-Karlik area, eastern segment of Chinese Tianshan Belt

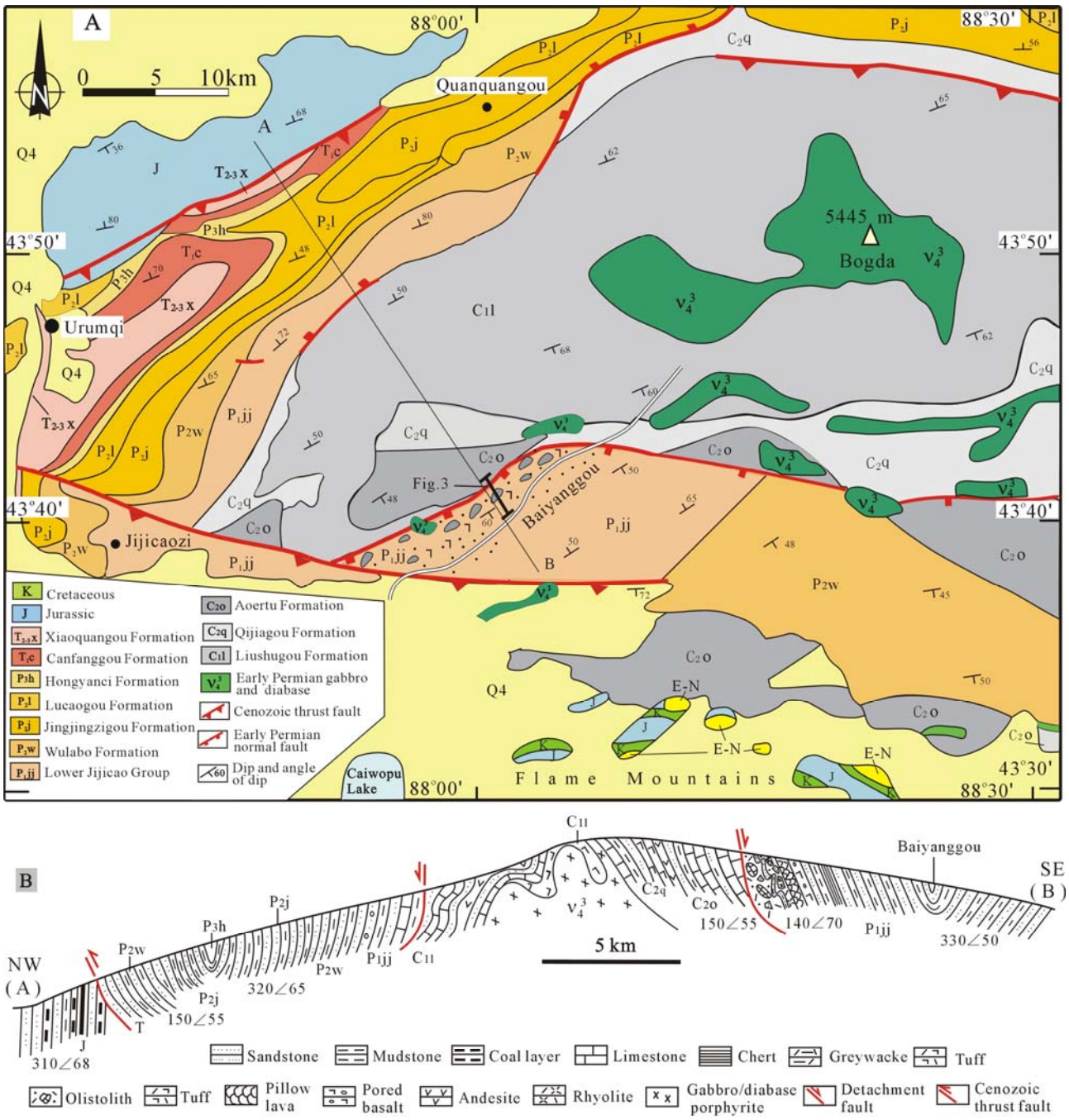

Figure 2. Geological map and cross-section of the Bogda area, northern Xinjiang

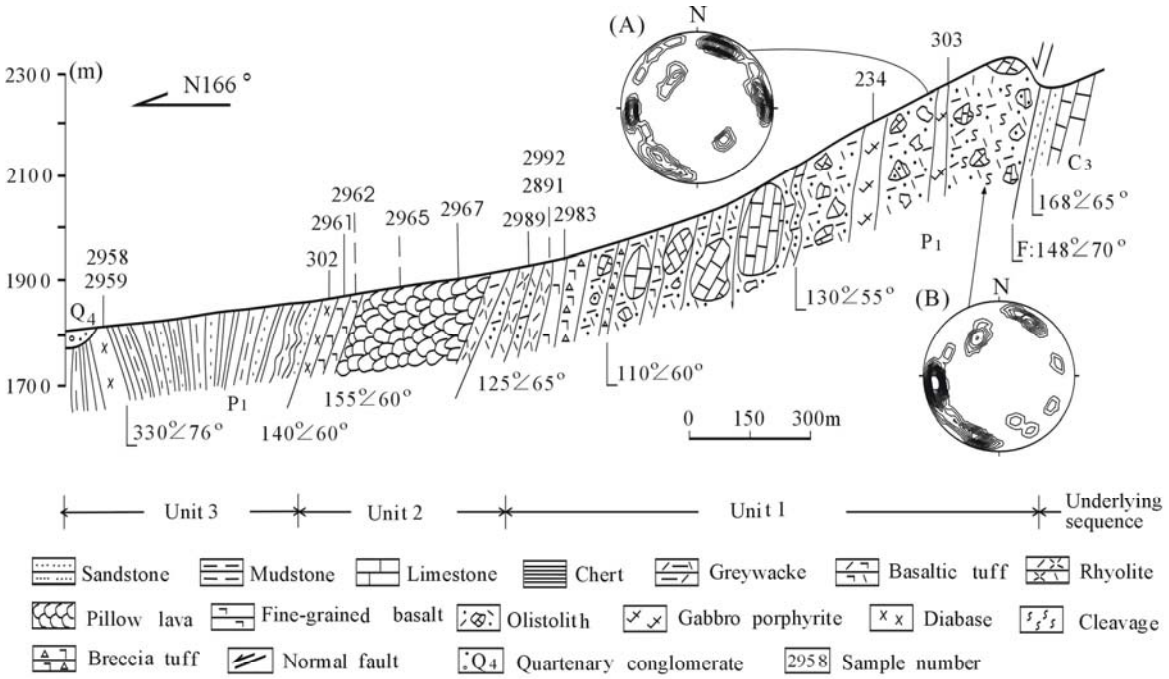

Figure 3. A geological cross-section showing three lithotectonic units of the southern Baiyanggou area. Stereographic projections (equal-area net, lower hemisphere) show the direction of the joints occurring in the olistostrome formation

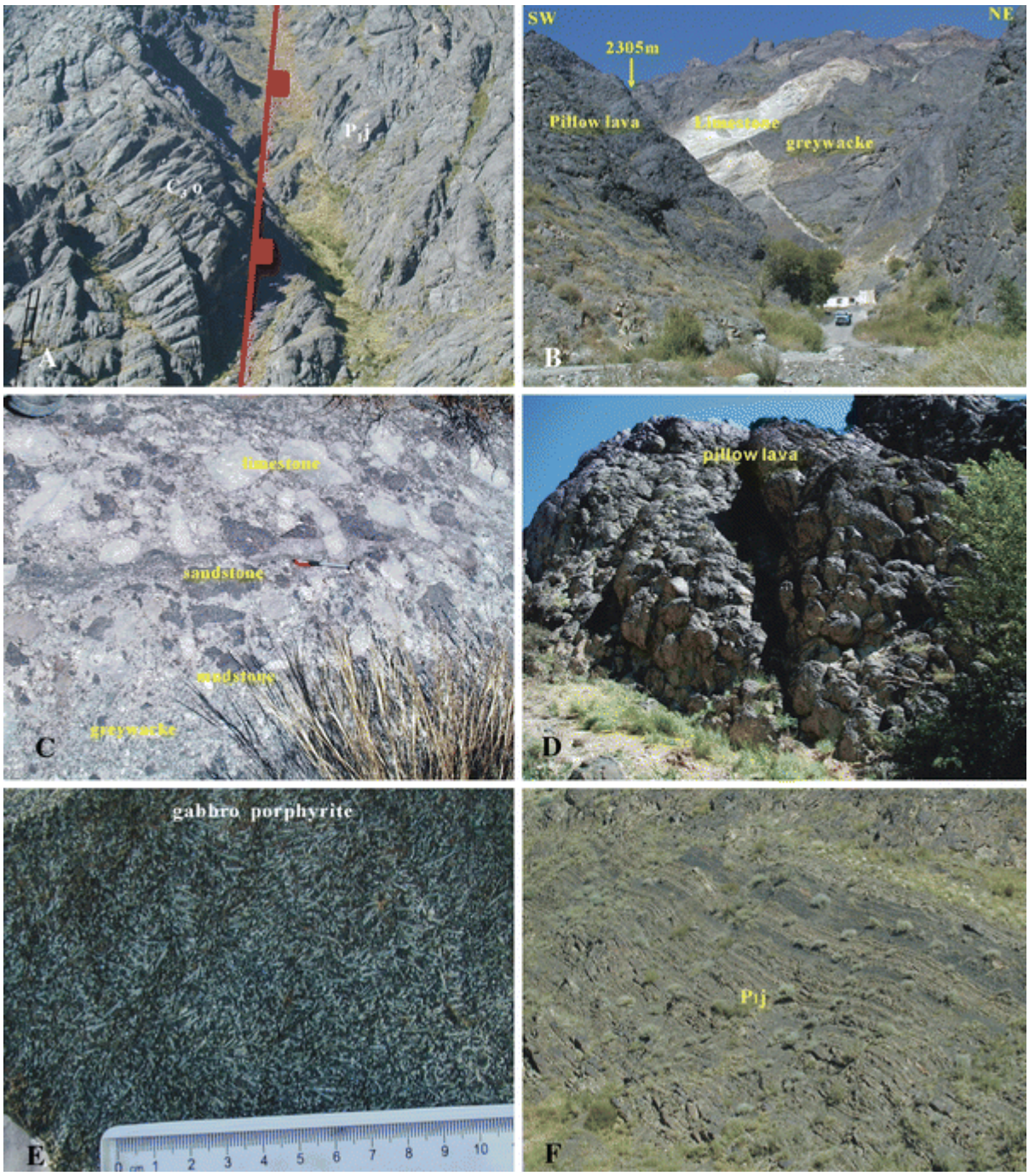

Figure 4. Field photographies of the olistostrome domain in the Baiyanggou area

A, Detachment fault between the Permian olistostrome and the Carboniferous limestone-sandstone; B, Olistolith of limestone (white) within greywacke matrix; C, Olistolith of limestone (ligh color); D, Pillow basalt; E, Gabbro porphyrite; F, Turbidite

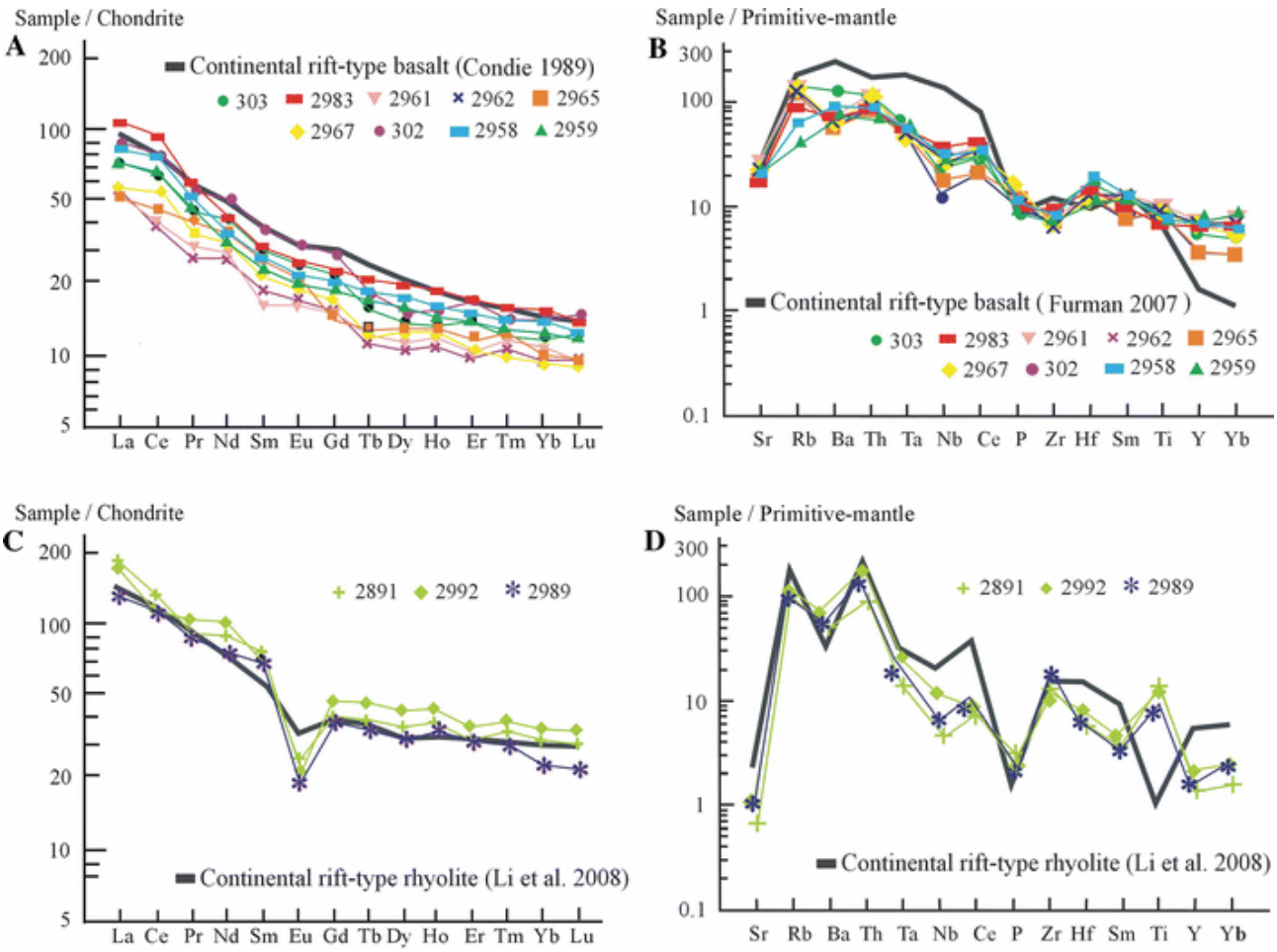

Figure 5. The Condrite-normalized REE patterns (A and C) and the primitive mantle-normalized trace elements spider diagrams (B and D) for the basalt and rhyolite, respectively

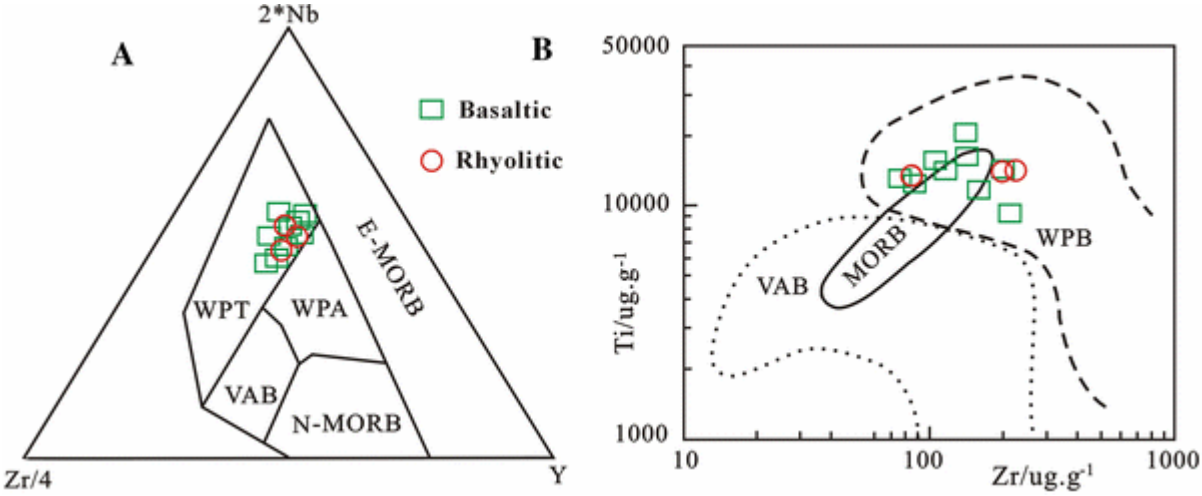

Figure 6. Tectonic discriminations of the Baiyanggou igneous rocks (Pearce et al. 1984)

A, The 2*Nb-Zr/4-Y diagram; B, The Ti vs Zr diagram

N-MORB, Normal Middle Ocean Ridge Basalt; E-MORB, Enriched Middle Ocean Ridge Basalt; WPT, Within-plate tholeiite; MORB, Middle ocean ridge basalt; WPB, Within-plate basalt; VAB, Volcanic arc basalt.

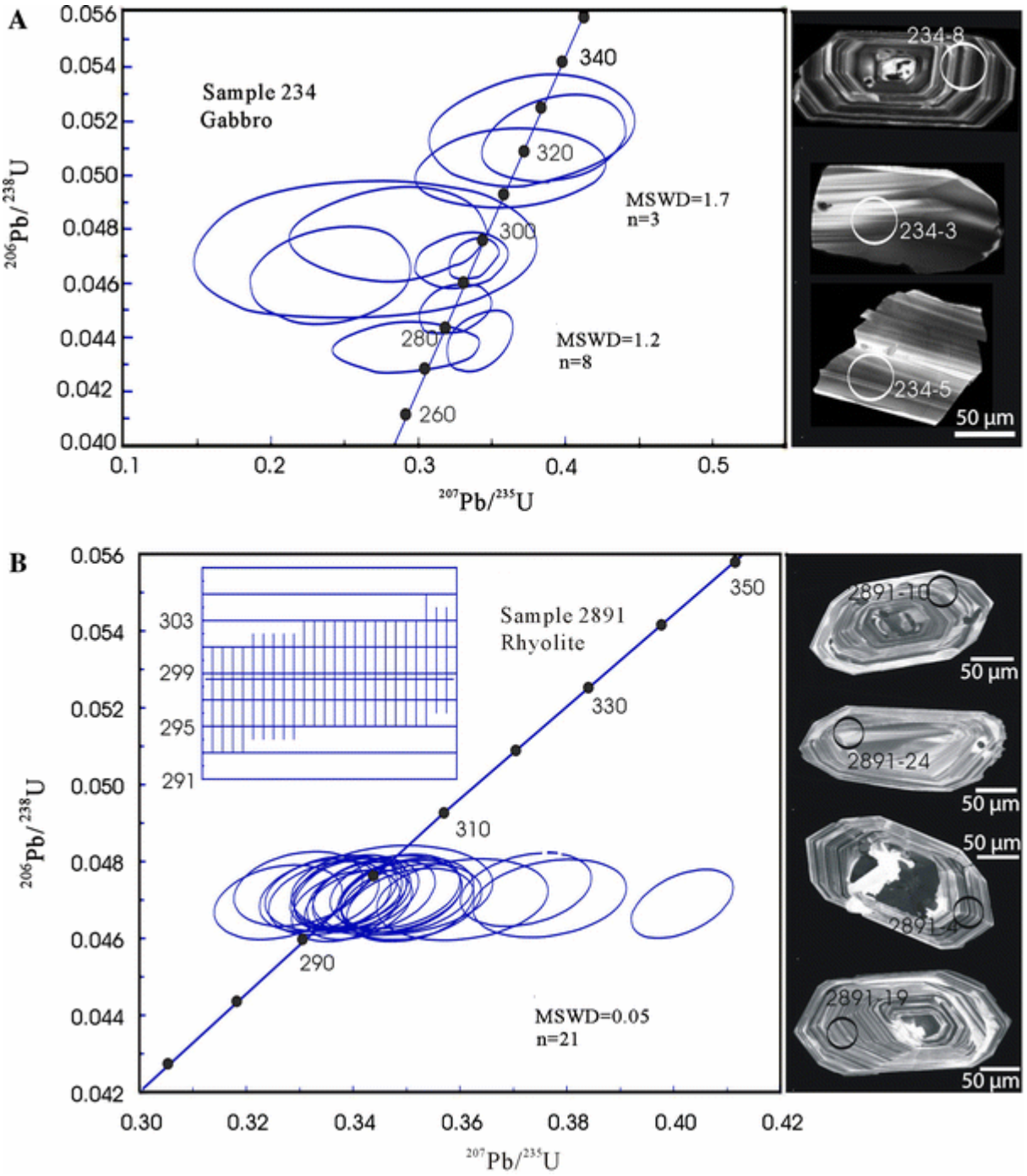

Figure 7. Concordia diagrams of zircon U-Pb dating on the igneous rocks of the Baiyanggou domain, representative CL images of dated zircons are also shown

A, Sample 234, gabbro porphyrite (SHRIMP); B, Sample 2891, rhyolite (LA-ICP-MS)

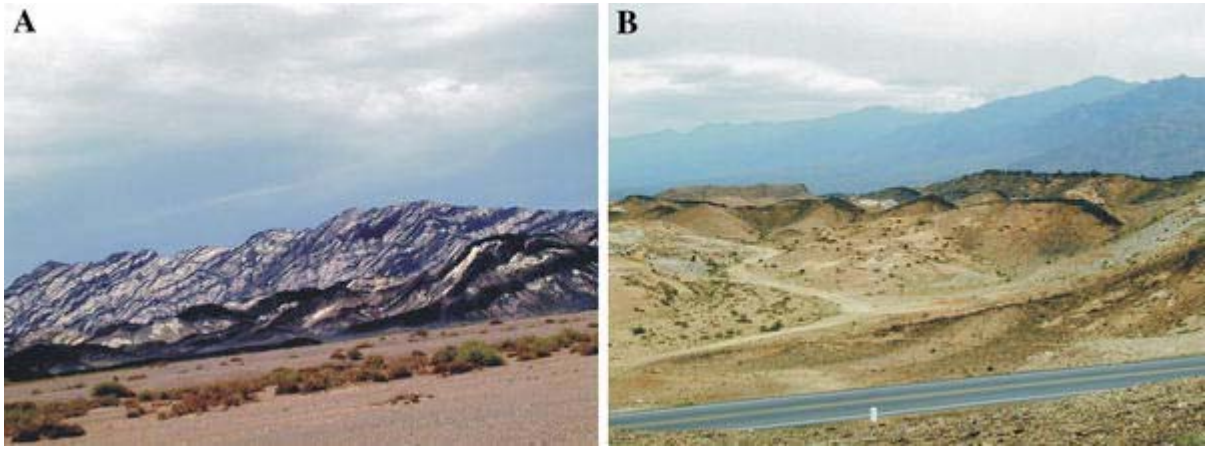

Figure 8. Images of Early Permian bimodal igneous rocks

A, The “zebra mountain” consisting of bimodal igneous rock swarm (Kuruqtag, Yuli County); B, the Early Permian mafic rock swarms intruding the Late Carboniferous granite (Weiya, Hami City)

Captions of tables

Table 1 Petrographic features of igneous rocks in the Baiyanggou, south of Urimqi City, NW China

Table 1 Petrographic features of magmatic rocks in the Bauyanggou of Urimqi, Xinjiang

Sample	303	2891	2992	2989	2983	2961
Location	Unit 1					
Texture	medium grained, gabbroic	porphyritic	porphyritic	porphyritic	porphyritic	porphyritic
Structure	massive	rhyolitic	rhyolitic	rhyolitic	massive, pore	massive, amygdale
Mineralogy	olivine (1-3%)+ monoclinic pyroxene (20%)+ labrador (35%)+ hornblende (15%); altered minerals (20-30%); chlorite+ hornblende; accessory minerals: magnetite (3%)	phenocrysts: potash feldspar+ sanidine (15%), quartz (25%),albite (5%), biotite (5%) groundmass: quartz+ albite (30%) scaly-like sericite (15-20%) accessory minerals: zircon+titanite (1-3%)	phenocrysts: potash feldspar+ sanidine (20%), quartz (25%),biotite (5%); groundmass (45-50%): quartz+ albite+ grasses accessory minerals: zircon+titanite+aptite (2-4%)	phenocrysts: potash feldspar+ sanidine (20%), quartz (20-25%),biotite (2-5%); groundmass (55-60%): quartz+ albite+ grasses accessory minerals: zircon+titanite+aptite (rare)	phenocryst: olivine (2-3%); pyroxene (5-10%);+labrador (15%), groundmass (75-80%): feldspar+ pyroxene+ hornblende; accessory minerals: magnetite+spinel (rare)	phenocryst: pyroxene (5%), labrador (10-15%); aphanitic groundmasses (75-80%): feldspar+ pyroxene+ hornblende+chlorite; amygdale: quartz+prehnite (3-5%)
Name	Gabbro	Rhyolite	Rhyolite	Rholite	Basalt	Basalt
Sample	2962	2965	2967	302	2958	2959
Location		Unit 2			Unit 3	
Texture	porphyritic	porphyritic	fine grained	fine grained, gabbroic	porphyritic	porphyritic, aphanophyric
Structure	pillow, amygdale	pillow, amygdale	massive, amygdale	massive	massive	massive
Mineralogy	phenocryst: olivine (3%); pyroxene (8%), labrador (15%); aphanitic groundmasses (70-75%): feldspar+ pyroxene+ hornblende; amygdale: quartz+prehnite (5-8%)	phenocryst: olivine (3%); pyroxene (5%), labrador (10-15%); aphanitic groundmasses (70-75%): feldspar+ pyroxene+ hornblende; altered minerals: chlorite (5%); amygdale: quartz+prehnite (3-5%)	fine grained aggregates (85-90%) of pyroxene,labrador and hornblende; altered minerals: chlorite (10%); amygdale: quartz+prehnite (2-5%); accessory minerals: magnetite (1-2%)	olivine (1-3%)+ pyroxene (30-35%)+ labrador (40-45%)+ hornblende (10%); altered minerals (15-20%): chlorite+ sericite+ calcite	phenocryst: pyroxene (5-10%), labrador (15-20%); microcrystal groundmasses (70-75%): feldspar+ pyroxene+ hornblende; accessory minerals: magnetite (1-3%)	phenocryst: pyroxene (10%), labrador (20%); microcrystal groundmasses (70%): feldspar+ pyroxene+ hornblende; accessory minerals: magnetite (3-5%)
Name	Pillow basalt	Pillow basalt	Basalt	Diabase	Diabase porphyrite	Diabase porphyrite

Table 2 Analytical results of major elements (wt%), rare earth elements (ppm) and trace elements (ppm) for igneous rocks from the Baiyanggou cross-section in the southern foot of Bogda Shan

Table 2 Analytical results of major elements (wt%), rare earth elements (ppm) and trace elements (ppm) for igneous rocks from the Baiyanggou cross-section in the southern foot of Bogda Shan

			Major elements (Wt%)														
Unit	Sample	Rock	SiO2	TiO2	Al2O3	Fe2O3	FeO	MnO	MgO	CaO	Na2O	K2O	P2O5	IL	Total	ANKC	
1	303	Gabbro	50.22	1.16	15.39	4.70	8.08	0.17	6.58	8.32	2.85	1.08	0.27	1.24	100.06	0.73	
1	2891	Rhyolite	72.48	0.27	12.58	2.63	0.86	0.26	1.26	2.25	2.47	4.64	0.13	0.34	100.17	0.96	
1	2992	Rhyolite	72.26	0.36	12.08	2.53	0.86	0.13	0.66	2.18	2.84	5.28	0.08	0.88	100.14	0.84	
1	2989	Rhyolite	71.13	0.21	12.48	2.36	1.02	0.09	0.58	1.13	3.52	5.56	0.08	0.85	99.01	0.9	
1	2983	Basalt	50.48	1.96	15.35	3.77	6.28	0.20	7.03	8.56	3.58	0.95	0.35	1.85	100.36	0.67	
2	2961	Basalt	51.43	2.09	15.37	4.35	7.38	0.13	6.35	8.52	2.86	0.93	0.23	1.04	100.68	0.73	
2	2962	Basalt	52.08	1.82	14.76	5.16	6.73	0.16	7.25	8.38	2.36	1.02	0.18	0.86	100.76	0.73	
2	2965	Pillow lava	52.68	1.87	14.25	3.54	6.31	0.24	7.12	7.52	3.67	0.92	0.29	2.35	100.76	0.68	
2	2967	Pillow lava	52.17	2.03	14.71	3.73	6.58	0.18	6.65	8.11	3.81	1.05	0.25	1.08	100.35	0.65	
2	302	Diabase	49.68	1.38	15.25	4.79	8.41	0.18	6.86	8.46	2.62	0.83	0.24	1.13	99.83	0.74	
3	2958	Diabase	51.76	0.85	16.02	4.55	6.48	0.12	6.42	7.16	4.08	1.13	0.33	1.06	99.96	0.77	
3	2959	Diabase	52.06	1.85	15.84	5.28	4.06	0.12	5.87	6.86	4.46	1.68	0.38	1.18	99.64	0.73	
			Rare earth elements (μg/g)														
Unit	Sample	Rock	La	Ce	Pr	Nd	Sm	Eu	Gd	Tb	Dy	Ho	Er	Tm	Yb	Lu	Total	Eu/Eu*
1	303	Gabbro	18.24	40.60	4.71	15.51	4.54	1.48	4.53	0.58	3.66	0.86	2.64	0.37	2.34	0.33	100.38	0.99
1	2891	Rhyolite	36.68	76.35	11.22	32.44	10.65	0.75	9.59	1.55	10.59	2.83	6.21	1.44	5.82	0.70	206.79	0.22
1	2992	Rhyolite	37.81	81.06	10.75	30.57	9.86	0.64	8.98	1.68	9.24	2.46	5.83	1.22	5.39	0.67	206.15	0.20
1	2989	Rhyolite	34.32	72.93	11.69	32.62	11.75	1.32	8.46	1.61	8.72	2.12	5.73	1.11	5.46	0.63	198.45	0.39
1	2983	Basalt	23.57	63.68	7.42	22.57	5.74	1.57	6.01	0.63	5.32	1.26	3.49	0.63	3.47	0.44	145.78	0.79
2	2961	Basalt	24.79	52.22	7.66	22.35	5.66	2.14	7.09	0.95	6.02	1.49	3.38	0.59	3.68	0.43	138.44	1.03
2	2962	Basalt	24.43	51.75	6.89	20.73	6.32	2.13	6.76	0.87	5.55	1.27	3.15	0.56	3.35	0.44	134.20	0.99
2	2965	Pillow lava	23.47	58.36	7.15	21.35	7.16	2.35	5.23	0.83	5.68	1.42	3.62	0.67	3.26	0.51	141.06	0.96
2	2967	Pillow lava	24.65	61.13	6.77	24.24	6.12	1.85	5.63	0.77	5.32	1.38	2.90	0.81	3.62	0.44	145.60	0.95
2	302	Diabase	18.55	39.57	5.62	15.23	4.85	1.64	4.88	0.62	3.79	0.84	2.39	0.35	2.27	0.33	100.89	1.02
3	2958	Diabase	26.46	49.54	6.52	22.32	5.14	1.65	5.48	0.72	5.24	1.26	3.13	0.50	2.58	0.41	130.95	0.94
3	2959	Diabase	17.39	58.03	6.75	20.74	5.56	1.68	5.66	0.83	4.72	1.21	2.72	0.58	2.97	0.43	129.26	0.91
			Trace elements (μg/g)														
Unit	Sample	Rock	Ti	Rb	Sr	Zr	Nb	Ba	Ce	P	Hf	Ta	Th	Sm	Y	Yb	U	V
1	303	Gabbro	15685	49.76	328.13	106.35	20.51	186.87	40.596	2124	4.88	1.49	1.99	4.54	22.12	2.34	0.89	146.74
1	2891	Rhyolite	14126	168.48	75.12	163.47	38.44	1026.6	76.346	89	13.56	2.25	26.35	10.65	41.68	5.82	1.56	65.22
1	2992	Rhyolite	12863	194.26	56.89	192.68	36.57	878.79	81.056	136	11.14	2.17	25.27	9.86	42.68	5.39	1.39	73.33
1	2989	Rhyolite	12356	189.24	70.29	245.48	39.62	898.56	72.928	243	12.87	2.49	19.36	11.75	41.22	5.46	3.22	76.46
1	2983	Basalt	13486	38.79	365.77	85.35	28.12	185.46	39.126	2106	4.15	1.51	2.73	5.42	30.14	2.49	0.79	151.77
2	2961	Basalt	13212	35.23	412.22	76.89	28.35	178.75	52.223	1846	3.90	1.24	3.21	5.66	25.48	3.68	1.11	168.46
2	2962	Basalt	12542	41.16	408.46	89.46	26.73	196.76	51.748	1678	4.65	1.36	2.69	6.32	24.86	3.35	1.25	158.84
2	2965	Pillow lava	11435	36.87	376.53	82.46	27.67	178.23	51.126	2526	3.92	1.33	2.88	5.87	29.24	2.86	1.02	146.35
2	2967	Pillow lava	10752	38.34	382.53	86.33	30.14	184.26	48.342	2612	4.14	1.11	3.135	5.73	28.72	2.69	1.40	138.216
2	302	Diabase	14246	46.35	368.25	116.25	20.23	205.65	39.568	1986	5.23	1.62	3.03	4.85	21.35	2.27	0.87	145.83
3	2958	Diabase	10246	31.34	342.42	89.36	28.32	235.45	49.538	1546	4.84	1.39	2.79	5.14	29.43	2.58	0.73	144.45
3	2959	Diabase	9682	25.35	293.43	125.43	26.74	217.45	58.034	1648	5.32	1.64	2.49	5.56	28.68	2.97	0.88	148.77

Table 3 The SHRIMP U-Pb data of zircons from the gabbro porphyrite in the Baiyanggou section

Grain no.	$^{206}Pb_c$ (%)	U ($\mu g.g^{-1}$)	Th ($\mu g.g^{-1}$)	Isotope ratios								Age (Ma)	
				$^{232}Th/^{238}U$	$^{206}Pb^*$ ($\mu g.g^{-1}$)	$^{207}Pb/^{206}Pb$ Age (Ma)	Error ±1σ	$^{207}Pb^*/^{235}U$ Age (Ma)	Error ±1σ	$^{206}Pb^*/^{238}U$ Age (Ma)	Error ±1σ	$^{206}Pb/^{238}U$	Error ±1σ
234-1	0.86	216	150	0.71	8.84	0.0475	13	0.263	1.8	0.0471	2.3	297.8	±6.5
234-2	0.00	453	555	1.27	17.0	0.0566	2.5	0.3423	2.8	0.04383	1.0	278.9	±2.8
234-3	0.30	498	553	1.15	20.1	0.0533	2.5	0.329	3.9	0.04680	0.90	295.4	±2.6
234-4	0.35	632	530	0.87	23.8	0.0514	5.9	0.292	6.9	0.04363	0.86	276.4	±2.3
234-5	0.22	636	413	0.67	24.7	0.0541	2.3	0.325	3.2	0.04503	0.83	285.5	±2.3
234-6	0.47	307	275	0.92	13.7	0.0607	4.3	0.406	4.9	0.05164	1.3	323.2	±4.0
234-7	0.22	197	139	0.73	8.09	0.0444	8.2	0.281	9.7	0.04778	1.4	300.7	±4.2
234-8	--	196	179	0.94	8.70	0.0522	7.5	0.383	7.4	0.05168	1.6	323.7	±5.1
234-9	--	339	255	0.78	14.6	0.0499	6.2	0.363	7.1	0.05024	1.1	315.0	±3.5
234-10	--	841	688	0.85	33.9	0.0520	1.9	0.3372	2.0	0.04687	0.68	296.6	±2.0
234-11	--	438	20	0.05	123	0.12316	0.72	5.564	0.97	0.3273	0.64	1,826	±10
234-12	0.00	168	177	1.09	6.66	0.0377	9.0	0.241	9.2	0.04627	1.6	292.1	±4.5

Table 4 The LA-ICPMS U-Pb data of zircons from the rhyolite in the Baiyanggou section

Grain no.	Th* ($\times 10^{-6}$)	U* ($\times 10^{-6}$)	Th/U	Isotope ratios								Ages (Ma)							
				$^{207}Pb/^{206}Pb$	1σ	$^{207}Pb/^{235}U$	1σ	$^{206}Pb/^{238}U$	1σ	$^{232}Th/^{238}U$	1σ	$^{207}Pb/^{206}Pb$	1σ	$^{207}Pb/^{235}U$	1σ	$^{206}Pb/^{238}U$	1σ	$^{208}Pb/^{232}Th$	1σ
2891-1	41335	112987	0.37	0.0581	0.00148	0.37681	0.00949	0.04704	0.00067	0.37	0.01	534	57	325	7	296	4	254	10
2891-2	28991	75868	0.38	0.05389	0.00127	0.35013	0.00821	0.04712	0.00064	0.38	0.01	366	54	305	6	297	4	232	8
2891-3	28931	99650	0.29	0.05038	0.00123	0.32603	0.00792	0.04694	0.00064	0.29	0.01	213	58	287	6	296	4	232	9
2891-4	53606	101649	0.53	0.05331	0.00197	0.34731	0.01245	0.04725	0.00077	0.53	0.01	342	86	303	9	298	5	243	10
2891-5	56716	126660	0.45	0.05428	0.00121	0.35077	0.00785	0.04687	0.00063	0.45	0.01	383	51	305	6	295	4	250	9
2891-6	68955	151507	0.45	0.05267	0.00099	0.34235	0.00656	0.04714	0.00061	0.45	0.01	315	44	299	5	297	4	232	8
2891-7	50813	160643	0.316	0.05245	0.00102	0.33867	0.00672	0.04684	0.00061	0.316	0.01	305	45	296	5	295	4	247	8
2891-8	177863	283021	0.63	0.06211	0.00092	0.40163	0.00631	0.0469	0.00059	0.63	0.01	678	32	343	5	295	4	256	8
2891-9	15477	43756	0.35	0.05562	0.00167	0.36047	0.01061	0.04701	0.0007	0.35	0.01	437	68	313	8	296	4	239	10
2891-10	62677	190807	0.33	0.0525	0.00092	0.3407	0.00616	0.04707	0.0006	0.33	0.01	307	41	298	5	297	4	224	7
2891-11	80611	257314	0.31	0.05205	0.00095	0.33861	0.00634	0.04718	0.00061	0.31	0.01	288	43	296	5	297	4	239	8
2891-12	42840	96351	0.45	0.05422	0.00134	0.35099	0.00864	0.04695	0.00065	0.45	0.01	380	57	305	6	296	4	230	8
2891-13	134094	233022	0.57	0.0533	0.0009	0.34621	0.00606	0.04712	0.00059	0.57	0.01	342	39	302	5	297	4	265	9
2891-14	34755	124197	0.28	0.05175	0.00116	0.33563	0.00756	0.04705	0.00063	0.28	0.01	274	53	294	6	296	4	253	10
2891-15	67240	122412	0.55	0.05225	0.00114	0.33954	0.00745	0.04714	0.00062	0.55	0.01	296	51	297	6	297	4	252	9
2891-16	35022	119893	0.29	0.05345	0.00124	0.34787	0.00803	0.04722	0.00064	0.29	0.01	348	54	303	6	297	4	274	11
2891-17	32265	107083	0.3	0.05714	0.00124	0.37239	0.0081	0.04727	0.00063	0.3	0.01	497	49	321	6	298	4	296	11
2891-18	26197	104875	0.25	0.05173	0.00131	0.33637	0.00847	0.04717	0.00065	0.25	0.01	273	59	294	6	297	4	273	11
2891-19	37056	106629	0.35	0.05215	0.00108	0.33958	0.0071	0.04723	0.00062	0.35	0.01	292	48	297	5	297	4	256	9
2891-20	36753	86160	0.43	0.05329	0.00143	0.34642	0.00917	0.04715	0.00066	0.43	0.01	341	62	302	7	297	4	259	10
2891-21	39812	113242	0.35	0.05376	0.00115	0.34902	0.00751	0.04709	0.00062	0.35	0.01	361	49	304	6	297	4	254	9
2891-22	50995	108208	0.47	0.05137	0.00113	0.33367	0.00739	0.04712	0.00062	0.47	0.01	257	52	292	6	297	4	280	10
2891-23	45561	93222	0.49	0.05058	0.00123	0.32976	0.00796	0.04729	0.00064	0.49	0.01	222	58	289	6	298	4	267	10
2891-24	73682	155052	0.48	0.05277	0.00101	0.341	0.00665	0.04688	0.0006	0.48	0.01	319	45	298	5	295	4	272	9

*, Derived from comparison of average raw counts with standard GJ-1 in each run; **, Common Pb corrected based on Andersen (2002).